LIMNOLOGY and OCEANOGRAPHY

ASLO

Limnol. Oceanogr. 66, 2021, 1155–1167

doi: 10.1002/lno.11672

Trait-based approach using in situ copepod images reveals contrasting ecological patterns across an Arctic ice melt zone

Laure Vilgrain,[1,2*] **Frédéric Maps**,[2] **Marc Picheral**,[1] **Marcel Babin**,[2] **Cyril Aubry**,[2] **Jean-Olivier Irisson**,[1,†] **Sakina-Dorothée Ayata**[1,3,†]

[1]Sorbonne Université, CNRS, Laboratoire d'Océanographie de Villefranche (LOV), Villefranche-sur-Mer, France
[2]Takuvik Joint International Laboratory Université Laval-CNRS, Département de Biologie and Québec-Océan, Université Laval, Québec, Canada
[3]Institut de Systématique, Evolution, Biodiversité (ISYEB), Muséum national d'Histoire naturelle, CNRS, Sorbonne Université, EPHE, Paris, France

Abstract

Imaging techniques are increasingly used in ecology studies, producing vast quantities of data. Inferring functional traits from individual images can provide original insights on ecosystem processes. Morphological traits are, as other functional traits, individual characteristics influencing an organism's fitness. We measured them from in situ image data to study an Arctic zooplankton community during sea ice break-up. Morphological descriptors (e.g., area, lightness, complexity) were automatically measured on ~ 28,000 individual copepod images from a high-resolution underwater camera deployed at more than 150 sampling sites across the ice-edge. A statistically-defined morphological space allowed synthesizing morphological information into interpretable and continuous traits (size, opacity, and appendages visibility). This novel approach provides theoretical and methodological advantages because it gives access to both inter- and intra-specific variability by automatically analyzing a large dataset of individual images. The spatial distribution of morphological traits revealed that large copepods are associated with ice-covered waters, while open waters host smaller individuals. In those ice-free waters, copepods also seem to feed more actively, as suggested by the increased visibility of their appendages. These traits distributions are likely explained by bottom-up control: high phytoplankton concentrations in the well-lit open waters encourages individuals to actively feed and stimulates the development of small copepod stages. Furthermore, copepods located at the ice edge were opaquer, presumably because of full guts or an increase in red pigmentation. Our morphological trait-based approach revealed ecological patterns that would have been inaccessible otherwise, including color and posture variations of copepods associated with ice-edge environments in Arctic ecosystems.

Functional traits are any features—morphological, physiological, etc—measurable at the individual-level and affecting the fitness of the organism (Violle et al. 2007). They can be classified according to the ecological function that they influence, such as feeding, growth, reproduction, and survival (Litchman et al. 2013). Trait-based approaches appeared in plant ecology in the 70s (Grime 1974) and stated being used by aquatic ecologists in the early 2000s (Willby et al. 2000; Usseglio-Polatera et al. 2000; Benedetti et al. 2016; Martini et al. (in press)). Trait-based analyses are relevant in community ecology because an individual's set of traits given environment determines its success (Violle et al. 2007). Ecological interactions (predation, mutualism, etc.) happen between individuals, not between taxonomic groups. Therefore, using trait composition can simplify the analysis of ecosystem complexity by focusing on a few characteristics transcending taxonomic distinctions and impacting ecological strategies (Litchman et al. 2013). By studying the composition and distribution of individual traits in an ecosystem, its structure and dominant processes can emerge from individual properties (Kiørboe et al. 2018). In zooplankton communities, for example, body length can influence secondary productivity and feeding mode can modify nutrients and energy transfers (Hébert et al. 2017).

Brun et al. (2019) demonstrated that over the past 55 years, climate change has altered zooplankton-fueled carbon export

*Correspondence: laure.vilgrain@obs-vlfr.fr

Additional Supporting Information may be found in the online version of this article.

†Co-last authors.

by changing the distribution of large-bodied individuals. Their study quantitatively linked shifts in individual properties (body size) and ecosystem functioning (carbon cycling). It shows how modulation in trait composition due to anthropogenic or natural perturbations could impact the ability of ecosystems to provide goods and services to human societies (Mouillot et al. 2013). More generally, trait-based approaches represent a way to focus on continuous, quantitative descriptors of fitness components (size spectrum, feeding intensity, etc.) rather than a set of discrete species; these metrics can more easily highlight subtle gradients and rates of change. As recommended by Mcgill et al. (2006), with functional trait measurements ecology can move from research questions centered around "How many species and why?" to ones focused on "How much variation in traits and why?"

Our study aims to answer the latter question for the copepod community during ice break up in an Arctic environment using a statistical description of body shapes ("morphometrics," Caillon et al. 2018). Sea ice melt is the primary driver of the spring phytoplankton bloom (Perrette et al. 2011). This intense pulse of primary production is partly captured by zooplankton that convert it into energy-rich lipid stores, fueling the whole trophic network all year long (Berge et al. 2012). In Arctic environments, zooplankton communities are dominated by only a few copepod species. Many of them share ecological characteristics, like feeding mode and ontogenetic migration, while presenting a continuum of morphological traits, such as size or lipid content, which are key drivers of ecosystem functioning (Schmid et al. 2018; Renaud et al. 2018). As a hub of matter and energy, these copepods hold a key trophic position in arctic ecosystems and have a crucial role in the oceanic carbon pump because of their vertical migrations (Falk-Petersen et al. 2009; Turner 2015). By studying copepods with trait-based approaches, we aim to reveal new aspects of ecological processes occurring during the phytoplankton ice-edge spring bloom.

To achieve this objective, we sought to quantify individual traits of copepods. A powerful way to capture such traits is by analyzing in situ images (Picheral et al. 2010; Schmid et al. 2016). Modern devices can image thousands of individuals in their immediate environment while simultaneously measuring physical and biological variables like temperature or fluorescence. Morphological traits that bear on ecological functions can be directly measured from each individual, yielding quantitative information on anatomical aspects (size, shape or transparency), and allowing to infer physiological or behavioral status (e.g., presence of lipid stores, prey encounter rate through the volume occupied by tentacles of cnidarian; Schmid et al. 2018; Ohman et al. 2019). Indeed, morphological approaches have been shown to be an objective and practical way of explaining patterns of *functional* variability, in phytoplankton and fishes (Kruk et al. 2010; Caillon et al. 2018). We hypothesize that traits of copepods will vary between the eastern and western sides of Baffin Bay as a function of water mass properties and seasonality in the surface layer. To assess the environmental influence on copepod trait distribution, we will answer the following questions: (1) Which traits can be objectively quantified on individual copepods from in situ images? (2) Can we detect the influence of the spatio-temporal dynamics of ice melt and water mass properties on trait distribution? (3) What are the ecological implications of such variations?

Materials and methods

GreenEdge expedition in Baffin Bay

We collected image data in Baffin Bay, a marginal Arctic sea located between Greenland and Canada, that is characterized by typical pan-Arctic environmental gradients (Tang et al. 2004). Water masses in the east and west of the bay have different origins and properties, creating strong gradients and influencing sea-ice formation and melt (Fig. 1). The Bay is particularly sensitive to climate change, with significant warming of Atlantic waters and freshening of Arctic waters measured between 1916 and 2003 (Zweng and Münchow 2006). The GreenEdge campaign took place aboard the *CCGS Amundsen* in June and July 2016. The cruise's main objective was to study the fate of organic matter newly produced during the transition period of ice break-up in spring/summer. The 163 sampling stations considered in this study were distributed along seven longitudinal transects crossing the ice edge (Fig. 1).

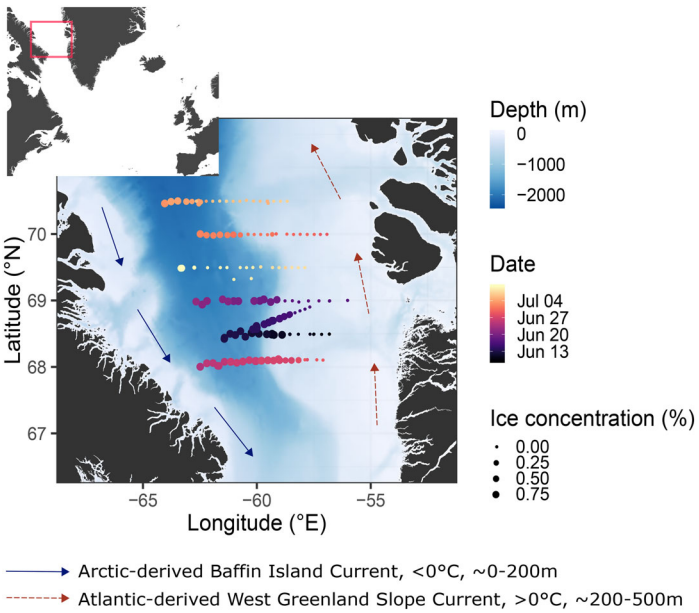

Fig. 1. Sampling map of the GreenEdge cruise across the ice edge in Baffin Bay. Baffin Bay is a marginal Arctic Sea where the southward-flowing Baffin current carries cold, low salinity waters (blue arrows). The northward-flowing West Greenland Slope Current carries warmer and saltier water originating in the Atlantic (red arrows). Each point on the map is a station colored according to the sampling date (between the 9th of June and the 10th of July) and of size proportional to the concentration of sea ice at the time of sampling.

Baffin Bay is covered by sea ice most of the year, except in August and September. In 2016, sea ice started to melt around the 10th of June in the sampling area and progressively disappeared, from east to west, at a rate of about 3.5 km d^{-1} (Randelhoff et al. 2019). As soon as snow on sea ice melts, and melt ponds form, the penetration of light allows for the start of primary production underneath it (Fortier et al. 2002; Arrigo et al. 2014; Oziel et al. 2019). Phytoplankton blooms generally develop a few days before (under sea ice) or after (in open waters) breakup (Randelhoff et al. 2019; Oziel et al. 2019). The sea ice gradually melted from east to west, illustrated by the strong east/west ice gradient along the three southern transects. However, by the time the ship navigated along transects, the three northern ones became almost ice-free (Fig. 1).

Sampling

In situ high-resolution imaging system: UVP5

The 5th version of the Underwater Vision Profiler (UVP5) was developed to image marine snow and zooplankton in situ and quantify their vertical distribution (Picheral et al. 2010). In the present study, it was mounted on the CTD-rosette so each image is associated with the environmental variables at coincident sampling locations. The UVP5 was set to acquire images at a frequency of 20 Hz which yields a typical sampling rate of 22.1 ± 9 images/m (∼ 1 image every 5 cm). Each 22 × 18 × 0.35 cm image sampled a 1.02 liter volume of seawater, with a resolution of 0.088 mm $pixel^{-1}$. The on-board computer automatically segmented and saved objects with an Equivalent Spherical Diameter (ESD) > 850 μm. Morphological descriptors (size, gray level distribution, etc.) were calculated for each object/individual in postprocessing with the ZooProcess software (Gorsky et al. 2010). Images, their metadata, and morphological descriptors were stored in the EcoTaxa web application (https://ecotaxa.obs-vlfr.fr/; Picheral et al. 2017). Morphological descriptors were used to train a random forest (RF) algorithm (Breiman 2001) that suggested a taxonomic classification for each object, which was then validated or corrected by a human annotator (the same user sorted 85% of the data but 9 others contributed). 1.2 M images were classified into 36 final categories (Supporting Information Table S1). Of these 1.2 M images, detritus, badfocus and fibers accounted for 96% of the data and are not considered here. The remain data is comprised of living organisms (45,883 images), of which 83% were copepods. We kept only copepod images taken in the surface layer described hereafter, where they accounted for more than 90% of organisms.

Environmental data

An instrument package containing a Conductivity-Temperature-Depth profiler (CTD, Seabird SBE-911), a Seapoint SCF fluorimeter, an oxygen optode (Seabrid, SBE 43) and a nitrate sensor (Satlantic, MBARI-ISUS) was deployed at each station to measure temperature (°C), potential temperature (°C), salinity (PSU), potential density (kg m^{-3}), dissolved oxygen concentration (ml L^{-1}), nitrate concentration (mmol m^{-3}), and chlorophyll *a* (Chl *a*) concentration (mg m^{-3}, estimated by fluorescence) (Lévesque et al., 2015; Bruyant et al., in prep.). Profile deepest points range between 117 and 2130 m, with a median depth of 360 m. All profiles were averaged at 1 m bin intervals to reduce noise. Spurious outliers were detected as anomalies to a moving median and removed. Missing values were inferred through an iterative Principal Component Analysis (Josse and Husson 2012). Several variables describing the structure of the water column were derived from each profile: pycnocline depth (depth of the maximum of the standard deviation calculated on a centered and weighted moving window of 41 m along the profile), stratification index (difference between the average value of the surface density at 2–5 m and at 40–50 m). At each station, 8–10 Niskin bottles collected water for phytoplanktonic pigment analysis. Sample depths were typically every 5 m between 0 and 30 m, and every 10 m between 30 and 100 m, though there was some minor variation between profiles. Pigments were extracted immediately after sampling, preserved, and quantified via High Performance Liquid Chromatography (HPLC) according to Ras et al. (2008). The depth of the sub-surface Chl *a* maximum (SCM) was then estimated from the HPLC data. Finally, we used ice concentration estimates derived from the AMSR2 satellite sensor data on a 3.125 km grid for each station location between 2016/03/01 and 2016/07/14 (Beitsch et al. 2014; Kaleschke and Tian-Kunze 2016).

We focused our study on the upper water column because (1) ice melt will mostly influence surface waters, (2) algal bloom occur in surface waters, (3) copepods are mostly located close to the surface to feed in the spring/summer period (Williams and Poulet 1986; Helaouët and Beaugrand 2007). We vertically segmented the water column by dividing the temperature profiles into six layers: warm surface layer, transition layer, cold intermediate layer, deep thermocline layer, deep cooling layer and deep stable layer (Fig. S1 for more details). Then, a PCA was performed on all planktonic concentrations obtained from UVP images in each layer to characterize the organismal distribution in the water column. Copepods were dominant close to the surface and were mainly associated with the three upper layers: warm, transition and cold intermediate layers (Fig. S1). Consequently, these layers were merged to define an ecologically coherent surface layer whose bottom is the depth of the cold intermediate layer; the deepest point where the temperature is 0.3°C warmer than the minimum of the profile. This surface layer has a mean depth of 101.7 m (min = 52 m, max = 227 m) and is systematically deeper in the Arctic-influenced and ice-covered part of the Bay. Finally, this layer always contains the sub-surface Chl *a* maximum.

Numerical analysis

Environmental gradients

To describe the physical and biogeochemical conditions in the surface layer, we carried out a PCA (Legendre and Legendre 2012) on: (1) temperature, salinity, oxygen, nitrate and

Chl *a* concentration averaged in the surface layer, (2) the variables derived to describe the structure of the water column (stratification index, pycnocline depth, sub-surface Chl *a* maximum (SCM) depth), (3) ice concentration (at the time of sampling and averaged over the cruise period), and (4) Open Water Days (OWD). OWD is the number of days a location has been free of ice (positive values) or, conversely how many days until the location thaws (negative values) (Randelhoff et al. 2019). After the PCA, the 163 stations were clustered by hierarchical classification carried out on the coordinates on the first three principal components, using a Euclidean distance and a synoptic Ward linkage (Murtagh and Legendre 2014). A threshold was set based on the aspect of the tree, hence defining groups of stations within which the aforementioned variables were homogeneous.

Construction of a multivariate morphological space from zooplankton images

To summarize the morphological characteristics of each object captured by the UVP, a *morphological space* was defined by performing a PCA on a selection of morphological descriptors (Supporting Information Table S2). The number of metrics for each trait were limited to 3–5 descriptors by removing correlated descriptors to avoid over-representing any particular aspect. All $\sim$ 28,000 copepods images located in the surface layer were used to construct this multivariate space. The descriptors were normalized by the Box-Cox transformation (Asar et al. 2017) to satisfy the conditions for PCA application. Axes were considered significant only if their associated eigenvalue was greater than the average of all the eigenvalues (Kaiser-Guttman criterion; Cattell 1966). The position of each plankton image in the space is thus a function of its morphology. To ease interpretation of the axes, example images were mapped to their position in the morphological space as follows: for each pair of principal components (i.e., PC1 vs PC2 or PC3 vs PC4) a grid was defined and eight images were randomly chosen and superposed at each node of the grid. The coordinates of this reduced morphological space (taking into account only the significant axes) are then used as synthetic, highly informative morphological traits for further analysis.

Traits and environmental gradients

To interpret variations of morphological traits along environmental gradients, objects coordinates on significant PC axes were averaged by station in the surface layer. Variations of traits in space were statistically interpolated by kriging. As each station belongs to one environmental cluster, it was also possible to compare values of traits between environmental clusters using a box plot representation, ANOVA and post-hoc statistical tests.

Numerical tools

All statistical analyses were conducted in the programming environment R 3.5.3 (R Core Team 2019). The package *castr* was used to clean vertical environmental profiles (https://github.com/jiho/castr), *car* for Box-Cox transformation (Weisberg and Fox 2018), F*actoMineR* (Lê et al. 2008) and *vegan* (Oksanen et al. 2007) for multivariate analysis, *tidyverse* (Wickham et al. 2019) for data manipulations and graphics, *morphr* (https://github.com/jiho/morphr) for images representation in the morphological space and finally *gstats* (Pebesma 2004) and *fields* (Nychka et al. 2017) for statistical interpolations. All data (including images) and codes are available in Supporting Information.

Results

Environmental gradients and seasonality

The first PCA on environmental variables revealed that PC1 is mostly structured by mean ice concentration, mean temperature and Open Water Days (Fig. 2). It separates cold, ice-covered waters to the west and warmer open waters to the east. PC2 has large, opposing contributions from pycnocline depth and stratification index, highlighting stations that are strongly stratified by the recent ice melt. Together, the principal components yielded three distinct clusters of stations. Stations from the western, ice covered, cluster are strongly influenced by the Baffin Current; nitrate concentration is high (> 8 mmol m^{-3}) and Chl *a* concentration is low. Stations from the eastern side, in open waters, are influenced by the relatively saltier and warmer Atlantic Current. At these stations, phytoplankton are abundant (high mean Chl *a* concentrations), the depth of the sub-surface Chl *a* maximum (SCM) increases from west to east (25–60 m), and nitrate concentration is relatively low indicating that the bloom is ending. The third cluster includes stations where ice has recently melted and are geographically spread along a central zone in the bay, larger on northern transects because of the timing of sampling (cf. Fig. 1). They are characterized by intermediate values of temperature, Chl *a*, and nitrate concentrations and a shallow Chl *a* maximum: the bloom is just starting, close to the surface.

Multivariate morphological space from zooplankton images

There were four significant axes describing the morphological space (Fig. 3). We assigned names to these four Principal Components to aid interpretation. We summarize the biological meaning of the various descriptors combined into one PC and define synthetic morphological traits. PC4, for example, broadly describes "complexity of shape/visibility of appendages" (Fig. 3b): bilateral symmetry is enhanced by visible antennae; circularity is higher when the prosome shape is not altered by visible appendages; gray levels variations are more important if there is contrast between the body and appendages; and so on. Image descriptors related to the organisms' size (e.g. *major* axis length, perimeter, area) contribute to PC1 and explain 36.4% of the variance (Fig. 3a). PC2 explains 25.9% of variance and is influenced by the opacity – how dark

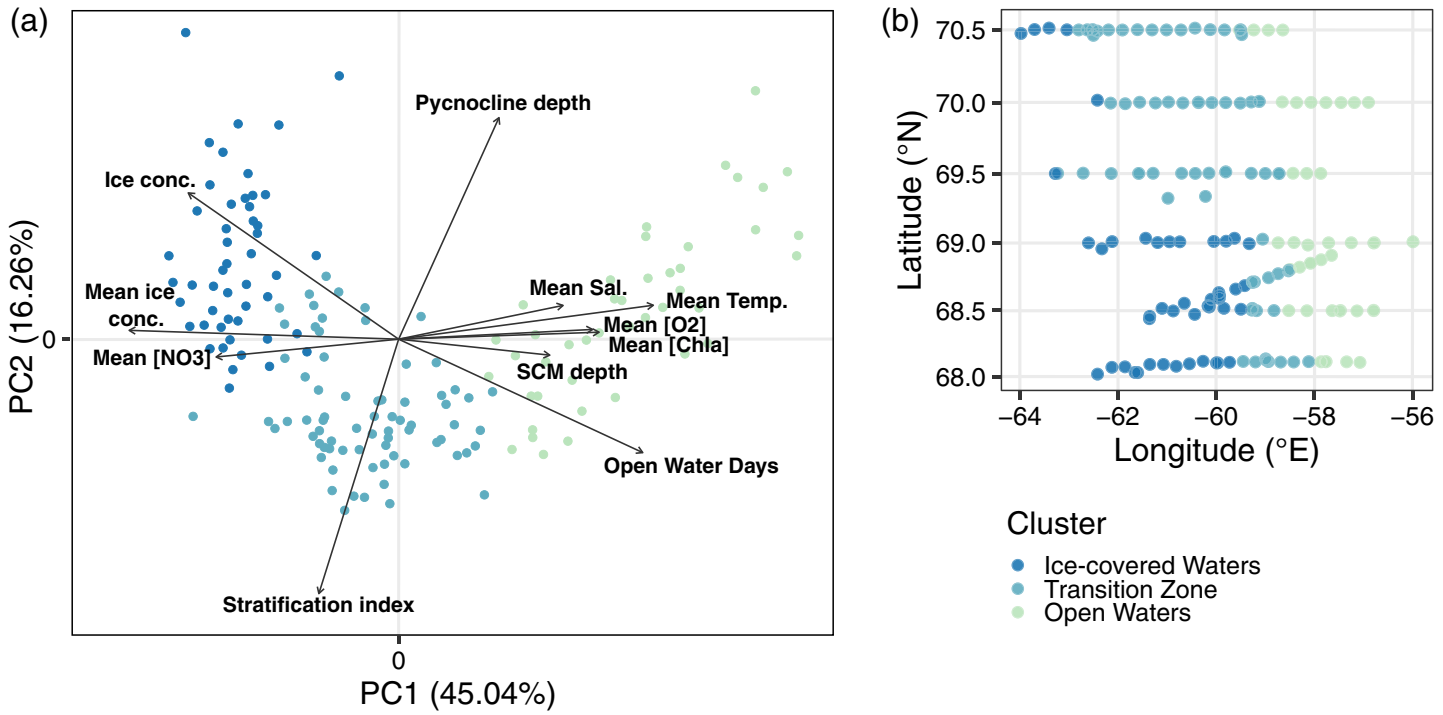

Fig. 2. Principal component analysis performed on environmental variables and clustering of stations. Coordinates of stations on the first three PCA axes were used for clustering (Euclidian distance, Ward method). Color indicates cluster membership in both PCA space (**a**) and Baffin Bay (**b**).

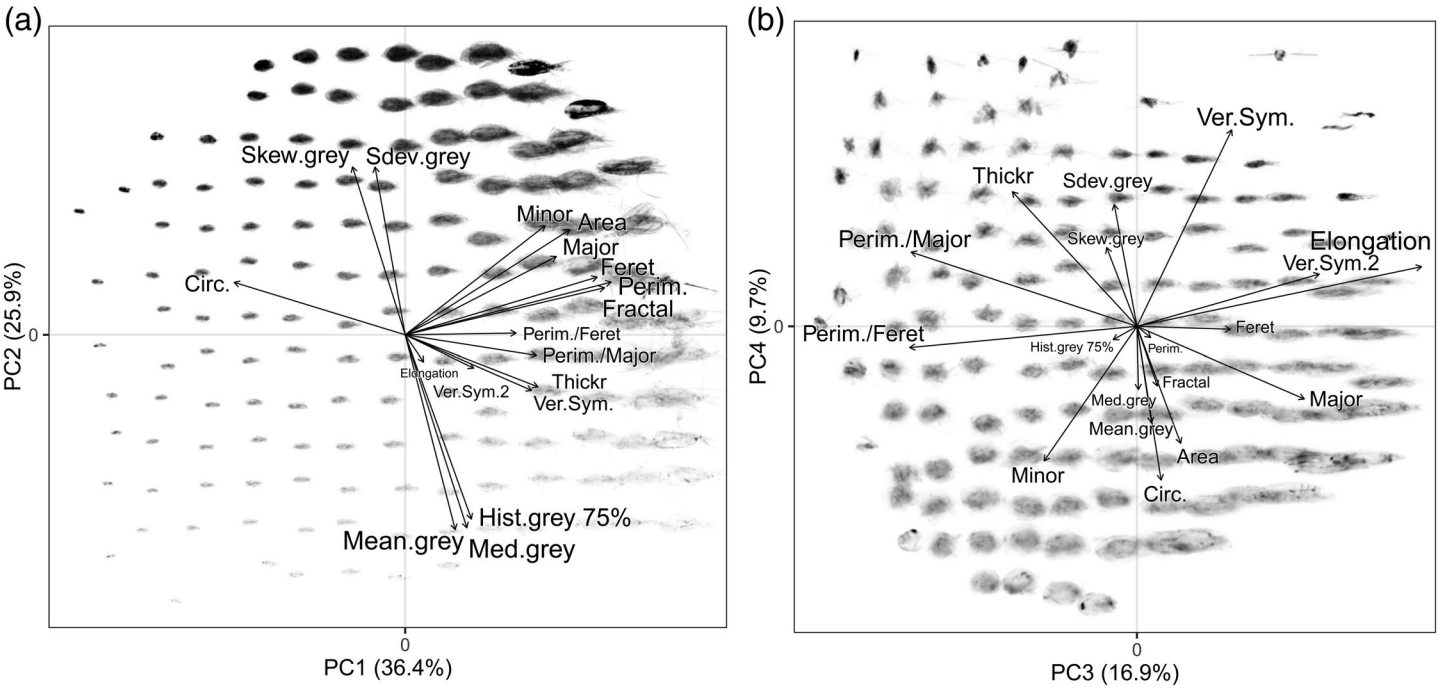

Fig. 3. Morphological space of copepods' UVP images. The four significant axes of a PCA performed on morphological descriptors are represented: PC1 and PC2 in (**a**), PC3 and PC4 in (**b**). For each factorial plane, morphotypes are represented according to their coordinates in the morphological space: A grid was defined and eight images close to the factorial plane considered were randomly selected, aligned and superimposed at each node of the grid for visualization. Definitions of morphological descriptors are presented in Table S2; code used to project images in the morphological space is available (*morphr* package, https://github.com/jiho/morphr).

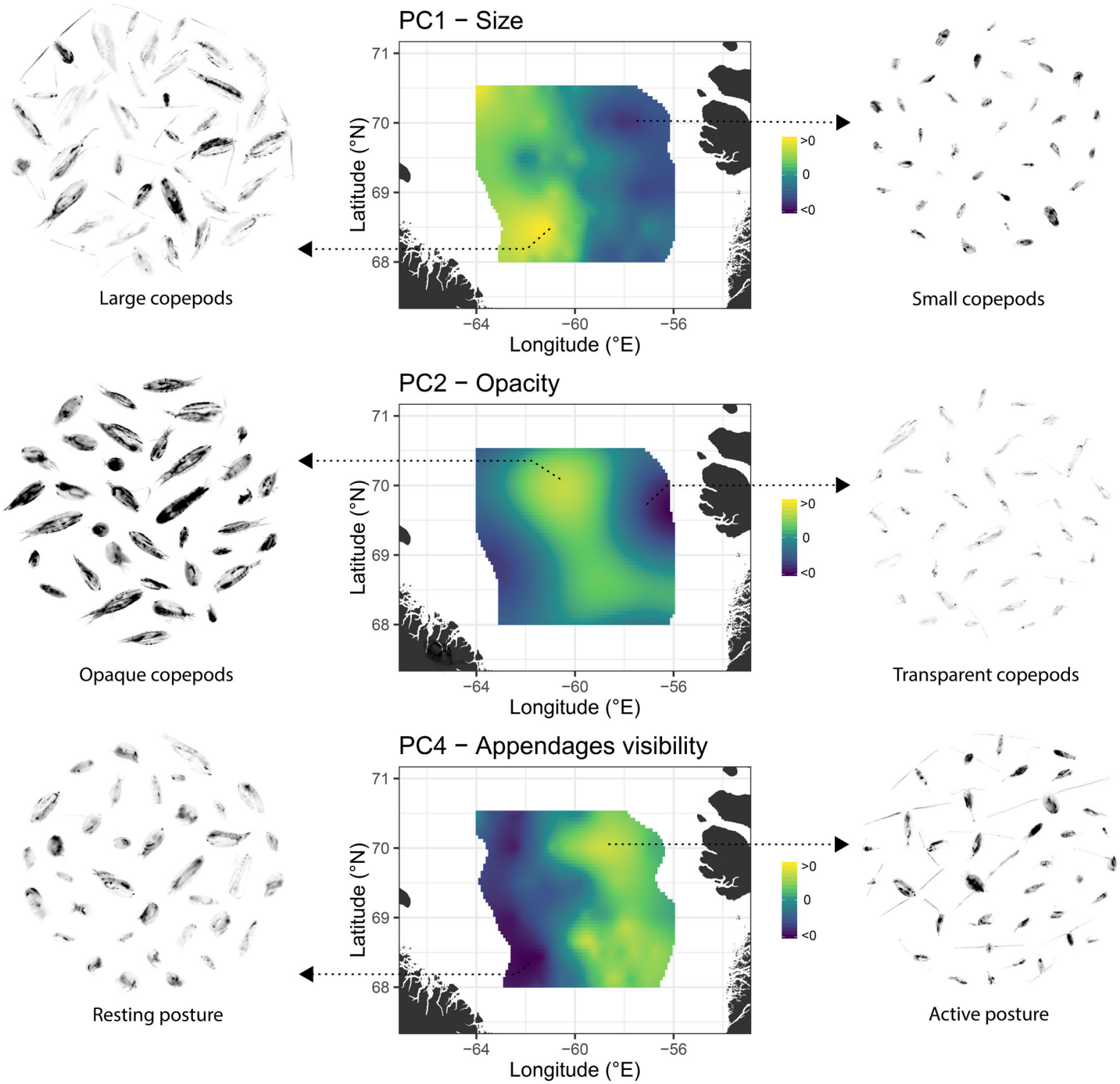

Fig. 4. Morphological traits distribution in Baffin Bay. Kriging of each station's average coordinates on PC1, PC2, and PC4 of copepods images from the surface layer. PC1 reflects individual size, PC2 opacity, and PC4 perimeter complexity (visibility of appendages). To illustrate "extreme" morphologies that drive the average PC value of a station, 36 images were randomly selected within the 10% highest or lowest along each PC and displayed on the sides.

they appear in UVP images—of organisms. PC3 (16.9% of variance) quantifies the elongation of the organisms (Fig. 3b). Finally, PC4 (9.7% of variance) was interpreted as the visibility of appendages, as explained above. In our dataset, variations of elongation (PC3) can be explained by copepods' orientation variability on images. A copepod imaged laterally or dorsally will appear longer (PC3 > 0) than a one seen from the front or the back (PC3 < 0). Although PC3 describes variations that are important within the dataset, we can make the reasonable assumption that orientation of individuals is either random or

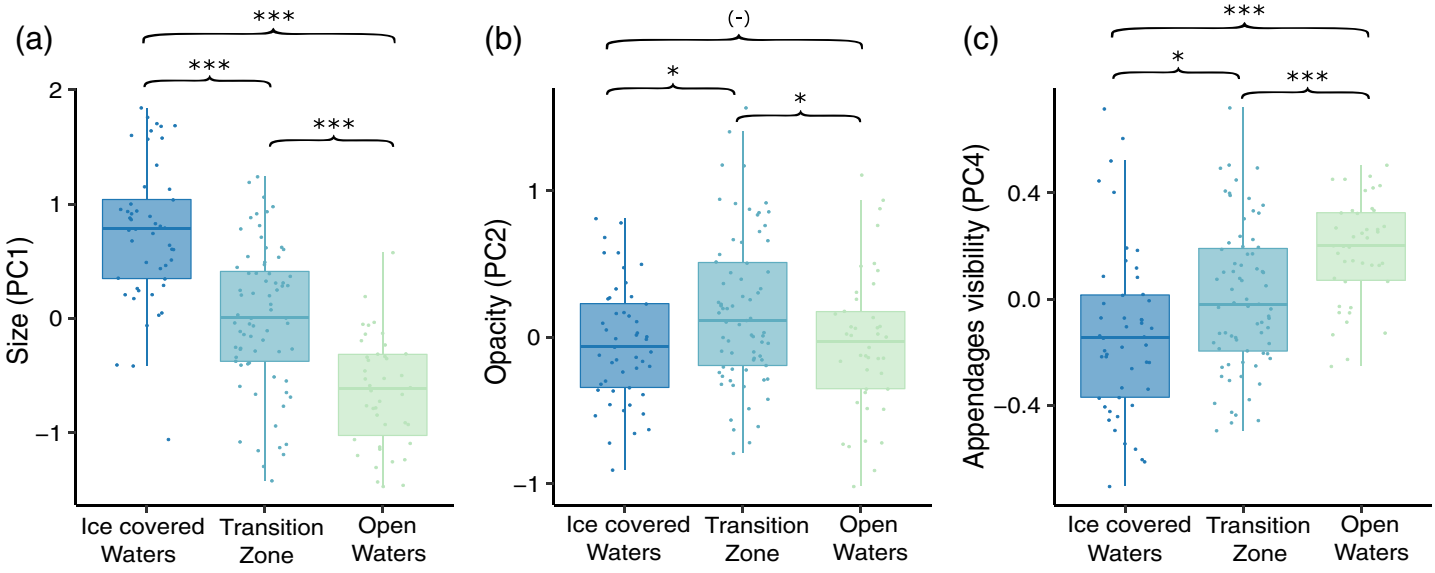

Fig. 5. Trait values according to environmental clusters. Box plots represent average trait values (a = size, b = opacity, c = appendages visibility) for each environmental cluster defined in Fig. 2. Each point represents the average value of the PC at a station. ANOVA identified significant differences between all PCs (PC1: $p < 0.001$; PC2: $p = 0.015$; PC4: $p < 0.001$) and the significance of post-hoc statistical tests is indicated symbolically on the figure (-: $p > 0.05$,*: $p < 0.05$, **: $p < 0.01$,***: $p < 0.001$).

slightly, but consistently, biased by the nominal flow generated by the UVP while sampling the water column. We will thus ignore PC3 for further analyses as there is no reason to link orientation relative to the camera with a specific ecological interpretation.

Distribution of morphological traits in Baffin Bay

The spatially interpolated PC values between each station revealed the spatial distribution of the size, opacity, and appendage visibility traits of copepods in Baffin Bay (Fig. 4). Since hundreds of images are available at each station, the computation of the mean value of each PC trait is statistically robust and allows us to illustrate the spatial distribution of dominant morphologies in the Bay. Copepods are typically larger (PC1) in western stations influenced by colder, fresher and ice-covered Arctic waters than in eastern stations where ice has already melted. Copepods present in the center of the Bay are generally opaquer in the UVP images as compared to copepods sampled at peripheral stations (PC2). Finally, it appears that more individuals have a complex perimeter with visible appendages in the east relative to western stations (PC4). In particular, large western copepods often have antennas folded along their body, whereas the smaller individuals in the east are imaged with extended antennae and pereiopods deployed.

Traits and environmental characteristics

The spatial patterns in copepod morphological traits are confirmed by one-way ANOVA and post-hoc tests on the average trait values according to the environmental clustering (Fig. 5). Size (PC1) and appendage visibility (PC4) differ significantly between the three clusters with a gradient from western to eastern clusters (Fig. 5a,c). Water temperature and ice concentration were the most important factors influencing the environmental clustering and could impact the size distribution. Appendage visibility (PC4) is significantly higher at the transition zone and in open waters where phytoplankton are present. Finally, the opacity of copepods (PC2, Fig. 5b) is significantly higher in the transition zone characterized by recent ice melt and a shallow bloom.

Discussion

Benefits of morphological trait-based approach from individual in situ images

We combined individual-based imagery and multivariate statistical analysis to implement a morphological trait-based approach to zooplankton ecology. The combination of these techniques allowed us to analyze many more profiles ($N = 163$) than would be possible with conventional net or pump sampling. The acquisition of large datasets—typically thousands of images per cast—enabled statistically robust descriptions of trends of morphological traits. This novel description of the ecosystem allowed us to infer community structure and functioning from individual properties. Moreover, this approach offers a continuous representation of traits, which has benefits in comparison to discrete traits especially for further numerical analyses (Mcgill et al. 2006).

In our study, the four significant PC axes of our morphological space explained 90% of the variance of the numerical descriptors of individual images and showed clear signals along environmental gradients. The ever-increasing production of images for plankton ecology paves the way for morphological trait-based studies that should provide original insights on ecosystem functioning. Many imaging devices already use morphological features to perform taxonomical classification of individuals (IFCB, Sosik and Olson 2007; FlowCam, Sieracki et al. 1998; LOKI, Schmid et al. 2016; ZooScan, Gorsky et al. 2010; Zooglider, Ellen et al. 2019). Freshwater and marine plankton morphology measured with such image processing methods could be easily analyzed using our approach.

The actual outcome of such analyses is highly dependent on the pixel resolution of the imaging system. In this study, we analyzed images of large Arctic zooplankton with a recent version of the Underwater Vision Profiler (Picheral et al. 2010). The instrument produces detailed high-resolution images of plankton at that size scale which makes the necessary morphological feature extraction possible. Systematic analyses should be performed using other devices and in other biogeographic regions to quantify the resolution bias of this morphological approach.

Size distribution as indicator of community structure

Our study aimed to elucidate patterns of morphological traits of copepods as a function of sea-ice dynamics (ice melt, ice-edge bloom, etc.). Results showed a strong west/east size gradient of the copepod community in Baffin Bay. Mean sizes are higher in Arctic-influenced and ice-covered waters than in ice-free and Atlantic-influenced waters. The consistent shift in size distribution is related to a change in the dominance of certain size classes; a complementary analysis of the spatial distribution of size (from PC1) showed elevated abundances of small individuals at eastern stations (Supporting Information, Fig. S2).

Therefore, our results allow us to propose two main hypotheses: size distribution may be linked to (1) the composition of communities advected by the currents, with small *Calanus finmarchicus* (~ 2–3 mm) dominating Atlantic waters, *C. hyperboreus* (up to 8 mm) being more abundant in Arctic waters (Beaugrand 2002); (2) the development of smaller copepodite life stages in ice-free and Chl *a* rich waters of the eastern Baffin Bay.

The UVP recorded images of copepods ranging from ca. 0.7–7 mm along the major axis, sizes typical of the dominant large Arctic species. However, the image resolution is not sufficient to distinguish copepod species and development stages precisely. Based on the taxonomic analysis of complementary vertical net sampling (Supporting Information Fig. S3), the most likely species encountered in this size range are *Calanus hyperboreus*, *C. glacialis*, *C. finmarchicus*, *Metridia longa* and adult stages of *Pseudocalanus* spp. (Sameoto 1984; Forest et al. 2012). *Oithona similis* and *Microcalanus sp.*, typical Arctic zooplankton species, are too small to be captured in UVP images.

Net sampling revealed that adult abundances, possibly reflecting the composition of advected communities, are not very different from west to east. Only *C. glacialis* and *C. finmarchicus* adults were counted in slightly higher numbers in the eastern, Atlantic-influenced part of the Bay. *C. hyperboreus*, *M. longa*, and *Pseudocalanus* adults are homogeneously spread out among stations (Fig. S3). The most striking element is that nauplii and young copepod stages from all *Calanus* species (Fig. S3b,c,f) are much more abundant in eastern Baffin Bay, which supports our second hypothesis. The strong size gradient is mostly caused by high recruitment of young copepod stages in response to sea ice melt and subsequent primary production pulse (Fig. 5). Indeed, *C. glacialis* and *C. finmarchicus* are mainly income breeders whose spawning is stimulated by Chl *a* concentration (Conover and Huntley 1991; Niehoff et al. 1999; Søreide et al. 2010). *C. hyperboreus* copepodites are also much more abundant in the east, but they are in late stages of development (no C1, some C2 and many C3 stages) because this capital breeder species spawns earlier in the season (Hirche and Niehoff 1996).

Variation of opacity: A reactive response to ice melt?

The transition zone between the ice-covered and open waters in the east (Fig. 2) was dominated by copepods that were opaquer (Fig. 4). We can expect that particles in the digestive tract are a major source of opacity. This is consistent with the observation that stations with the highest integrated Chl *a* concentration were also the areas of highest copepod opacity, particularly along the ice edge (Lafond et al., 2019). On the contrary, stations with low phytoplankton abundances and high phaeopigment concentrations (post-bloom conditions, Lafond et al. 2019) show weaker opacities.

A copepod's gut content is sometimes clearly distinguishable in UVP images (see Fig. 6, 1a). It is not, however, the only colored structure visible on images. Red light illumination is used by several in situ imaging devices, including the UVP, because these wavelengths are known to reduce phototactic behavior of zooplankton (Cohen and Forward 2002). Raw UVP images of red objects will appear bright over a dark background. The pixel values in the images we worked with were inverted for practical reasons (Picheral et al. 2010) so that reddish areas appear dark. In UVP images from this study, localized darker regions are visible within the anterior ventral zone, the basis of pereiopods, antennas and at the posterior extremity of the lipid sac (Fig. 6, 1b). Calanoid copepods usually concentrate astaxanthin, an antioxidant carotenoid pigment that they metabolize from precursors found in phytoplanktonic preys (Lotocka 2004). These pigments are good quenchers of oxygen-free radicals and can prevent lipid peroxidation (Hairston 1976; Miki 1991; Lotocka 2004; Weaver et al. 2018). Even if the role of pigmentation is rather well-known, there is still a lack of information on how it

varies according to environmental conditions. Relatively high quantity and good quality of phytoplankton are necessary for copepods to successfully transform phytoplanktonic precursors into antioxidant pigments (Andersson et al. 2003). This metabolism could reduce the potential oxidative stress caused by solar radiation in near-surface blooms when the ice cover breaks up, and help maximize copepod survival, which requires large lipid reserves for their maturation (Hylander et al. 2015).

A third possible explanation of the observed opacity variation is related to reproduction phenology since reproductive structures, such as gonads and eggs, are also very pigmented (Fig. 6, 1c). *C. finmarchicus* and *C. glacialis* depend mainly on the spring bloom to produce eggs, so their reproductive structures are likely to be mature and visible in females (Niehoff et al. 1999). Nevertheless, clearly identifying these structures in images captured in the surface layer was quite rare (about 10% of a random subsample of 150 images), while the occurrence of noticeable gut content and red pigments was much more common.

Unexpected indices of in situ feeding activity

The PC4 in our analysis revealed distinct patterns of appendage visibility in our images that we did not expect to resolve so clearly. Images with low score values on this axis often show copepods that have their antennae folded alongside their body. Lenz and Roncalli (2019) have interpreted this posture as a sign of diapause. More generally, the pose can be interpreted as the morphological signature of a rather inactive behavior, as also demonstrated from Zooglider images (Ohman 2019). Likewise, images with high PC4 values were typically of copepods that had appendages extended out of their body. In the Arctic, most copepods are "feeding-current feeders" (Marshall 1973; Barton et al. 2013): they create a current with their pereiopods to entrain particles and phytoplankton cells (Kiørboe 2011), while their antennae are spread out. We therefore hypothesize that the mean score value of PC4 for a sub-part of the community (here, copepods of the surface layer) is an indicator of the feeding activity of the community (Fig. 6, 2a,b).

It follows that maximal feeding intensity occurs in the eastern part of the Bay, where phytoplankton concentrations are

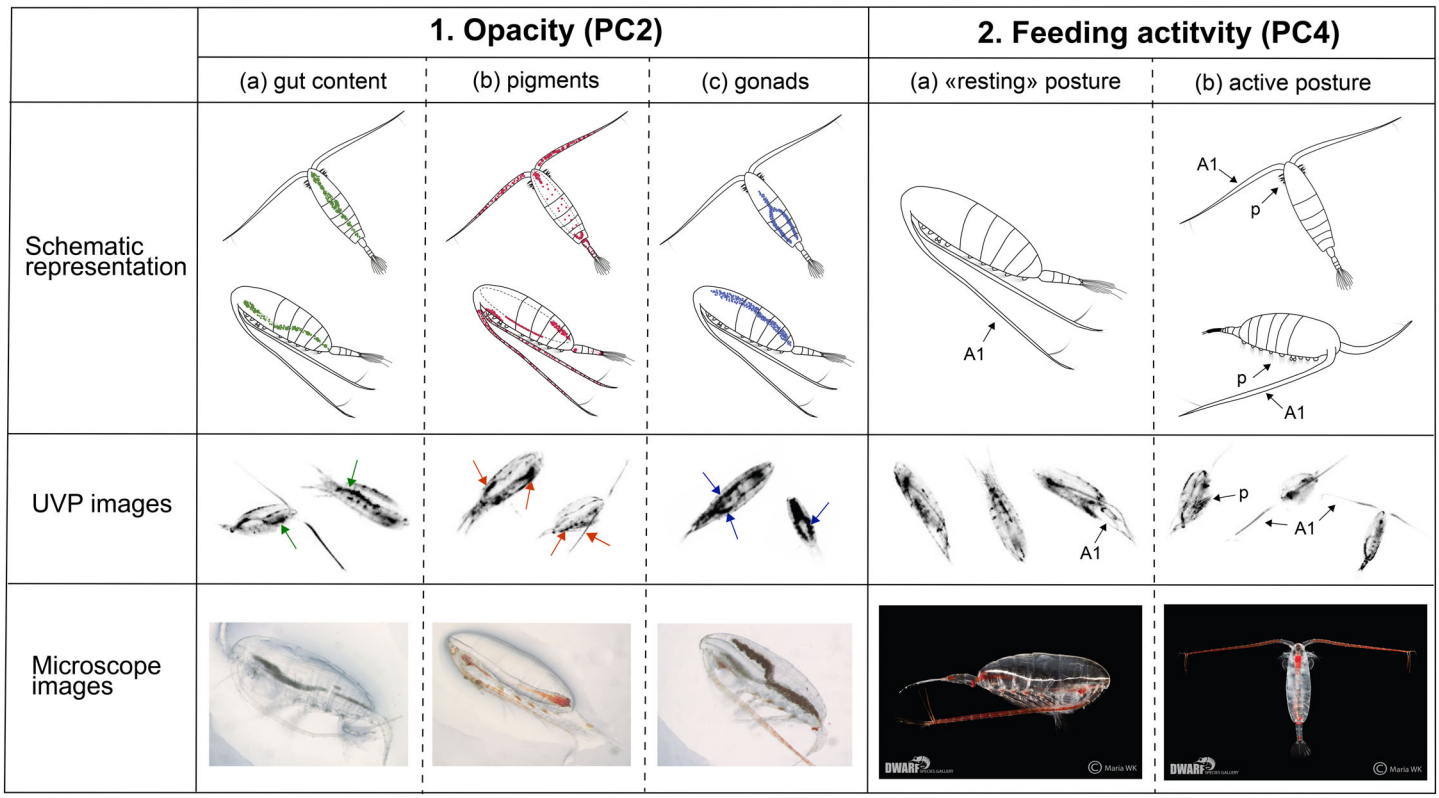

Fig. 6. Illustration of opacity and feeding activity variations visible on copepods (*C. hyperboreus*) schemes, UVP images and stereo-microscope images. Opacity characterized by PC2 score can be linked to gut content (1a), red pigments (1b), or gonads (1c), and often a combination of the three. PC4 scores capture appendage extension and are potentially indicators of copepod feeding activity: Individuals in a resting posture have antennae (A1) along their body (2a), active filter-feeding copepods extend their antennae (A1) and sometimes pereiopods (p) deployed (2b). Stereo-microscope images illustrating opacity variations were taken by Geneviève Perrin (Institut des Sciences de la Mer, Université du Québec, Rimouski, Canada); those illustrating feeding activity were taken by Maria Włodarska-Kowalczuk (Institute of Oceanology, Polish Academy of Sciences, Poland, http://www.iopan.gda.pl/projects/Dwarf/species_gallery/crustacea.html).

the highest. Small and "active" copepods could be copepodites development stages hatched in spring, whose filtration activity is highest to ensure their development and successful overwintering. The stations with high Chl *a* concentration (81.5 +/− 29 mg m^{-2}) and many pelagic diatoms (185,00 to 624,000 cells L^{-1}) were ice-free stations situated on the eastern part of transects 69°N and 70°N, close to the ice edge (Lafond et al. 2019). These stations also present a high PC4 mean value, which was expected since Arctic copepods and diatoms have a well-known prey–predator relationship (Scott et al. 2002).

Conclusions

Our morphological trait-based analysis of UVP images highlights the strong response of the surface copepod community to ice melt and phytoplankton dynamics. We mostly find non-feeding and large (adult) copepods in ice-covered waters, while ice break-up and increase of Chl *a* concentrations are associated with: (1) a large increase of small *Calanus sp*. stages abundances; (2) the pigmentation of copepods at the ice edge due to full gut content and astaxanthin accumulation; and (3) elevated feeding activity in open waters, as inferred from copepod posture.

References

Andersson, M., L. Van Nieuwerburgh, and P. Snoeijs. 2003. Pigment transfer from phytoplankton to zooplankton with emphasis on astaxanthin production in the Baltic Sea food web. Mar. Ecol. Prog. Ser. **254**: 213–224. doi:10.3354/meps254213

Arrigo, K. R., D. K. Perovich, R. S. Pickart, et al. 2014. Phytoplankton blooms beneath the sea ice in the Chukchi Sea. Deep Sea Res. II: Top. Stud. Oceanogr. **105**: 1–16. doi:10.1016/j.dsr2.2014.03.018

Asar, Ö., O. Ilk, and O. Dag. 2017. Estimating Box-Cox power transformation parameter via goodness-of-fit tests. Commun. Stat.—Simul. Comput. **46**: 91–105. doi:10.1080/03610918.2014.957839

Barton, A. D., A. J. Pershing, E. Litchman, N. R. Record, K. F. Edwards, Z. V. Finkel, T. Kiørboe, and B. A. Ward. 2013. The biogeography of marine plankton traits. Ecol. Lett. **16**: 522–534. doi:10.1111/ele.12063

Beaugrand, G. 2002. Reorganization of North Atlantic marine copepod biodiversity and climate. Science **296**: 1692–1694. doi:10.1126/science.1071329

Beitsch, A., L. Kaleschke, and S. Kern. 2014. Investigating high-resolution AMSR2 sea ice concentrations during the February 2013 fracture event in the Beaufort Sea. Remote Sens. (Basel) **6**: 3841–3856. doi:10.3390/rs6053841

Benedetti, F., S. Gasparini, and S.-D. Ayata. 2016. Identifying copepod functional groups from species functional traits. J. Plankton Res. **38**: 159–166. doi:10.1093/plankt/fbv096

Berge, J., T. M. Gabrielsen, M. Moline, and P. E. Renaud. 2012. Evolution of the Arctic Calanus complex: An Arctic marine avocado? J. Plankton Res. **34**: 191–195. doi:10.1093/plankt/fbr103

Breiman, L. 2001. Random forests. Mach. Learn. **45**: 5–32. doi:10.1023/A:1010933404324

Brun, P., K. Stamieszkin, A. W. Visser, P. Licandro, M. R. Payne, and T. Kiørboe. 2019. Climate change has altered zooplankton-fuelled carbon export in the North Atlantic. Nature Ecol. Evolut. **3**: 416–423. doi:10.1038/s41559-018-0780-3

Caillon, F., V. Bonhomme, C. Möllmann, and R. Frelat. 2018. A morphometric dive into fish diversity. Ecosphere **9**: ecs2.2220. doi:10.1002/ecs2.2220

Cattell, R. B. 1966. The scree test for the number of factors. Multivar. Behav. Res. **1**: 245–276. doi:10.1207/s15327906mbr0102_10

Cohen, J. H., and R. B. Forward. 2002. Spectral sensitivity of vertically migrating marine copepods. Biol. Bull. **203**: 307–314. doi:10.2307/1543573

Conover, R. J., and M. Huntley. 1991. Copepods in ice-covered seas—Distribution, adaptations to seasonally limited food, metabolism, growth patterns and life cycle strategies in polar seas. J. Mar. Syst. **2**: 1–41. doi:10.1016/0924-7963(91)90011-I

Ellen, J. S., C. A. Graff, and M. D. Ohman. 2019. Improving plankton image classification using context metadata. Limnol. Oceanogr.: Methods **17**: 439–461. doi:10.1002/lom3.10324

Falk-Petersen, S., P. Mayzaud, G. Kattner, and J. R. Sargent. 2009. Lipids and life strategy of Arctic *Calanus*. Mar. Biol. Res. **5**: 18–39. doi:10.1080/17451000802512267

Forest, A., L. Stemmann, M. Picheral, L. Burdorf, D. Robert, L. Fortier, and M. Babin. 2012. Size distribution of particles and zooplankton across the shelf-basin system in southeast Beaufort Sea: combined results from an Underwater Vision Profiler and vertical net tows. Biogeosciences **9**: 1301–1320. doi:10.5194/bg-9-1301-2012

Fortier, M., L. Fortier, C. Michel, and L. Legendre. 2002. Climatic and biological forcing of the vertical flux of biogenic particles under seasonal Arctic Sea ice. Mar. Ecol. Prog. Ser. **225**: 1–16. doi:10.3354/meps225001

Gorsky, G., M. D. Ohman, M. Picheral, and others. 2010. Digital zooplankton image analysis using the ZooScan integrated system. J. Plankton Res. **32**: 285–303. doi:10.1093/plankt/fbp124

Grime, J. P. 1974. Vegetation classification by reference to strategies. Nature **250**: 26–31. doi:10.1038/250026a0

Hairston, N. C. 1976. Photoprotection by carotenoid pigments in the copepod *Diaptomus nevadensis*. Proc. Natl. Acad. Sci. **73**: 971–974. doi:10.1073/pnas.73.3.971

Hébert, M.-P., B. E. Beisner, and R. Maranger. 2017. Linking zooplankton communities to ecosystem functioning: Toward an effect-trait framework. J. Plankton Res. **39**: 3–12. doi:10.1093/plankt/fbw068

Helaouët, P., and G. Beaugrand. 2007. Macroecology of *Calanus finmarchicus* and *C. helgolandicus* in the North Atlantic Ocean and adjacent seas. Mar. Ecol. Prog. Ser. **345**: 147–165. doi:10.3354/meps06775

Hirche, H.-J., and Niehoff, B. 1996. Reproduction of the Arctic copepod *Calanus hyperboreus* in the Greenland Sea-field and laboratory observations. Polar Biol. **16**: 209–219. doi:10.1007/bf02329209

Hylander, S., T. Kiørboe, P. Snoeijs, R. Sommaruga, and T. G. Nielsen. 2015. Concentrations of sunscreens and antioxidant pigments in Arctic *C alanus* spp. in relation to ice cover, ultraviolet radiation, and the phytoplankton spring bloom: MAAs and astaxanthin in copepods. Limnol. Oceanogr. **60**: 2197–2206. doi:10.1002/lno.10194

Josse, J., and F. Husson. 2012. Handling missing values in exploratory multivariate data analysis methods. J. Soc. Franç. Stat. **153**: 79–99 hal-00811888.

Kaleschke, L., and X. Tian-Kunze. 2016. AMSR2 ASI 3.125 km Sea Ice Concentration Data, V0.1″, Institute of Oceanography, University of Hamburg, Germany, digital media (ftp-projects.zmaw.de/seaice/), [BEGIN 01/03/2016 - END 14/07/2016].

Kiørboe, T. 2011. How zooplankton feed: Mechanisms, traits and trade-offs. Biol. Rev. **86**: 311–339. doi:10.1111/j.1469-185X.2010.00148.x

Kiørboe, T., A. Visser, and K. H. Andersen. 2018. A trait-based approach to ocean ecology. ICES J. Mar. Sci. **75**: 1849–1863. doi:10.1093/icesjms/fsy090

Kruk, C., V. L. M. Huszar, E. T. H. M. Peeters, S. Bonilla, L. Costa, M. LüRling, C. S. Reynolds, and M. Scheffer. 2010. A morphological classification capturing functional variation in phytoplankton. Freshw. Biol. **55**: 614–627. doi:10.1111/j.1365-2427.2009.02298.x

Lafond, A., K. Leblanc, B. Quéguiner, and others. 2019. Late spring bloom development of pelagic diatoms in Baffin Bay. Elem. Sci. Anth. **7**: 44. doi:10.1525/elementa.382

Lê, S., J. Josse, and F. Husson. 2008. FactoMineR: An R package for multivariate analysis. J. Stat. Softw. **25**: 1–18. doi:10.18637/jss.v025.i01

Legendre, P., and L. Legendre. 2012. Chapter 9 - ordination in reduced space, p. 425–520. *In* Developments in environmental modelling. Elsevier.

Lenz, P. H., and V. Roncalli. 2019. Diapause within the context of life-history strategies in Calanid copepods (Calanoida: Crustacea). Biol. Bull. **237**: 170–179. doi:10.1086/705160

Lévesque, K., S. Morisset, T. Linkowski, and J. Zier. 2015. CCGS Amundsen Navigation (NAV) data recorded during the annual science expeditions in the Canadian Arctic.doi:10.5884/12447

Litchman, E., M. D. Ohman, and T. Kiørboe. 2013. Trait-based approaches to zooplankton communities. J. Plankton Res. **35**: 473–484. doi:10.1093/plankt/fbt019

Lotocka, M. 2004. Changes in carotenoid composition in different developmental stages of copepods: *Pseudocalanus acuspes* Giesbrecht and *Acartia* spp. J. Plankton Res. **26**: 159–166. doi:10.1093/plankt/fbh021

Marshall, S. M. 1973. Respiration and feeding in copepods, p. 57–120. *In* Advances in marine biology. Elsevier.

Martini, S., F. Larras, B. Aurélien, and others. (in press). Functional trait-based approaches as a common framework for aquatic ecologists. Limnol. Oceanogr.

Mcgill, B., B. Enquist, E. Weiher, and M. Westoby. 2006. Rebuilding community ecology from functional traits. Trends Ecol. Evol. **21**: 178–185. doi:10.1016/j.tree.2006.02.002

Miki, W. 1991. Biological functions and activities of animal carotenoids. Pure Appl. Chem. **63**: 141–146. doi:10.1351/pac199163010141

Mouillot, D., N. A. J. Graham, S. Villéger, N. W. H. Mason, and D. R. Bellwood. 2013. A functional approach reveals community responses to disturbances. Trends Ecol. Evol. **28**: 167–177. doi:10.1016/j.tree.2012.10.004

Murtagh, F., and P. Legendre. 2014. Ward's hierarchical agglomerative clustering method: Which algorithms implement Ward's criterion? J. Classific. **31**: 274–295. doi:10.1007/s00357-014-9161-z

Niehoff, B., U. Klenke, H. Hirche, X. Irigoien, R. Head, and R. Harris. 1999. A high frequency time series at Weathership M, Norwegian Sea, during the 1997 spring bloom: The reproductive biology of *Calanus finmarchicus*. Mar. Ecol. Prog. Ser. **176**: 81–92. doi:10.3354/meps176081

Nychka, D., R. Furrer, J. Paige, and S. Sain. 2017. fields: Tools for Spatial Data, R package version 9.8-3, https://github.com/NCAR/Fields.doi:10.5065/D6W957CT

Ohman, M. D. 2019. A sea of tentacles: Optically discernible traits resolved from planktonic organisms in situ. ICES J. Mar. Sci. **76**: 1959–1972–1972. doi:10.1093/icesjms/fsz184

Ohman, M. D., R. E. Davis, J. T. Sherman, K. R. Grindley, B. M. Whitmore, C. F. Nickels, and J. S. Ellen. 2019. Zooglider: An autonomous vehicle for optical and acoustic sensing of zooplankton. Limnol. Oceanogr.: Methods **17**: 69–86. doi:10.1002/lom3.10301

Oksanen, J., F. G. Blanchet, R. Kindt, and others. 2007. The vegan package. Community ecology package **10**: 631–637.

Oziel, L., P. Massicotte, A. Randelhoff, and others. 2019. Environmental factors influencing the seasonal dynamics of spring algal blooms in and beneath sea ice in western Baffin Bay. Elem. Sci. Anth. **7**: 34. doi:10.1525/elementa.372

Pebesma, E. J. 2004. Multivariable geostatistics in S: The gstat package. Comput. Geosci. **30**: 683–691. doi:10.1016/j.cageo.2004.03.012

Perrette, M., A. Yool, G. D. Quartly, and E. E. Popova. 2011. Near-ubiquity of ice-edge blooms in the Arctic. Biogeosciences **8**: 515–524. doi:10.5194/bg-8-515-2011

Picheral, M., L. Guidi, L. Stemmann, D. M. Karl, G. Iddaoud, and G. Gorsky. 2010. The underwater vision profiler 5: An advanced instrument for high spatial resolution studies of particle size spectra and zooplankton: Underwater vision profiler. Limnol. Oceanogr.: Methods **8**: 462–473. doi:10.4319/lom.2010.8.462

Picheral, M., S. Colin, and J.-O. Irisson. 2017. EcoTaxa, a tool for the taxonomic classification of images. http://ecotaxa.obs-vlfr.fr.

R Core Team. 2019. R: A language and environment for statistical computing. R Foundation for Statistical Computing. http://www.R-project.org/

Randelhoff, A., L. Oziel, P. Massicotte, and others. 2019. The evolution of light and vertical mixing across a phytoplankton ice-edge bloom. Elem. Sci. Anth. **7**: 20. doi:10.1525/elementa.357

Ras, J., H. Claustre, and J. Uitz. 2008. Spatial variability of phytoplankton pigment distributions in the subtropical South Pacific Ocean: Comparison between in situ and predicted data. Biogeosciences **5**: 353–369. doi:10.5194/bg-5-353-2008

Renaud, P. E., M. Daase, N. S. Banas, and others. 2018. Pelagic food-webs in a changing Arctic: A trait-based perspective suggests a mode of resilience. ICES J. Mar. Sci. **75**: 1871–1881. doi:10.1093/icesjms/fsy063

Sameoto, D. D. 1984. Vertical distribution of zooplankton biomass and species in northeastern Baffin Bay related to temperature and salinity. Polar Biol. **2**: 213–224. doi:10.1007/bf00263627

Schmid, M. S., C. Aubry, J. Grigor, and L. Fortier. 2016. The LOKI underwater imaging system and an automatic identification model for the detection of zooplankton taxa in the Arctic Ocean. Methods Oceanogr. **15–16**: 129–160. doi:10.1016/j.mio.2016.03.003

Schmid, M. S., F. Maps, and L. Fortier. 2018. Lipid load triggers migration to diapause in Arctic Calanus copepods—Insights from underwater imaging. J. Plankton Res. **40**: 311–325. doi:10.1093/plankt/fby012

Scott, C., S. Kwasniewski, S. Falk-Petersen, and J. Sargent. 2002. Species differences, origins and functions of fatty alcohols and fatty acids in the wax esters and phospholipids of *Calanus hyperboreus*, *C. glacialis* and *C. finmarchicus* from Arctic waters. Mar. Ecol. Prog. Ser. **235**: 127–134. doi:10.3354/meps235127

Sieracki, C., M. Sieracki, and C. Yentsch. 1998. An imaging-in-flow system for automated analysis of marine microplankton. Mar. Ecol. Prog. Ser. **168**: 285–296. doi:10.3354/meps168285

Søreide, J. E., E. Leu, J. Berge, M. Graeve, and S. Falk-Petersen. 2010. Timing of blooms, algal food quality and *Calanus glacialis* reproduction and growth in a changing Arctic. Glob. Chang. Biol. **16**: 3154–3163. doi:10.1111/j.1365-2486.2010.02175.x

Sosik, H. M., and R. J. Olson. 2007. Automated taxonomic classification of phytoplankton sampled with imaging-in-flow cytometry. Limnol. Oceanogr. Methods **5**: 204–216. doi:10.4319/lom.2007.5.204

Tang, C. C. L., C. K. Ross, T. Yao, B. Petrie, B. M. DeTracey, and E. Dunlap. 2004. The circulation, water masses and sea-ice of Baffin Bay. Prog. Oceanogr. **63**: 183–228. doi:10.1016/j.pocean.2004.09.005

Turner, J. T. 2015. Zooplankton fecal pellets, marine snow, phytodetritus and the ocean's biological pump. Prog. Oceanogr. **130**: 205–248. doi:10.1016/j.pocean.2014.08.005

Usseglio-Polatera, P., M. Bournaud, P. Richoux, and H. Tachet. 2000. Biological and ecological traits of benthic freshwater macroinvertebrates: Relationships and definition of groups with similar traits. Freshw. Biol. **43**: 175–205. doi:10.1046/j.1365-2427.2000.00535.x

Violle, C., M.-L. Navas, D. Vile, E. Kazakou, C. Fortunel, I. Hummel, and E. Garnier. 2007. Let the concept of trait be functional! Oikos **116**: 882–892. doi:10.1111/j.0030-1299.2007.15559.x

Weaver, R. J., P. A. Cobine, and G. E. Hill. 2018. On the bioconversion of dietary carotenoids to astaxanthin in the marine copepod, *Tigriopus californicus*. J. Plankton Res. **40**: 142–150. doi:10.1093/plankt/fbx072

Weisberg, S., and J. Fox. 2018. An R companion to applied regression, Third ed. Sage.

Wickham, H., M. Averick, J. Bryan, and others. 2019. Welcome to the Tidyverse. J. Open Source Softw. **4**: 1686. doi:10.21105/joss.01686

Willby, N. J., V. J. Abernethy, and B. O. L. Demars. 2000. Attribute-based classification of European hydrophytes and its relationship to habitat utilization. Freshw. Biol. **43**: 43–74. doi:10.1046/j.1365-2427.2000.00523.x

Williams, R., and S. A. Poulet. 1986. Relationship between the zooplankton, phytoplankton, particulate matter and dissolved free amino acids in the Celtic Sea: I. Unstratified water conditions. Mar. Biol. **90**: 279–284. doi:10.1007/BF00569139

Zweng, M. M., and A. Münchow. 2006. Warming and freshening of Baffin Bay, 1916–2003. J. Geophys. Res. **111**: C07016. doi:10.1029/2005JC003093

Acknowledgments

The GreenEdge project was conducted under the scientific coordination of the CERC program and of the CNRS & Université Laval Takuvik Joint International Laboratory (UMI3376). This work is a contribution to the scientific program of Québec Océan. We thank officers and crew of CCGS Amundsen, Marie-Hélène Forget and Joannie Ferland for organizing the cruise, Céline Dimier and Josephine Ras for HPLC analyses, Pascal Guillot and the Amundsen Science Data team for the CTD data processing and quality control, and all other scientists and technicians who contributed to fieldwork. We also thank Achim Randelhoff for his expertise on water masses conditions in Baffin Bay. This work was funded mainly by our salaries as French or Canadian state employees and therefore by French and Canadian taxpayers. The Green Edge project is funded by the following

programs and agencies: the Network of Centres of Excellence ArcticNet, the Canada Foundation for Innovation (Amundsen Science), Canada's Excellence in Research Chair (CERC) program, the Natural Sciences and Engineering Research Council of Canada, ANR (Contract #111112), CNES (project #131425), French Arctic Initiative, Fondation Total, CSA, LEFE and IPEV (project #1164). Funding for this research was provided by the ARTIFACTZ and CARDINAL projects (Sentinelle Nord—Université Laval, Québec, Canada/Université Côte d'Azur, Nice, France/Arctic University of Norway, Tromsø, Norway). FM acknowledges the Fonds de Recherche Nature et Technologies du Québec for partial funding of a sabbatical in the Laboratoire d'Océanographie de Villefranche, France. SDA acknowledges the CNRS for her two sabbatical years as visiting researcher at ISYEB. Finally, we especially thank Eric Orenstein for his careful copy-editing and his relevant remarks on the manuscript.

Conflict of Interest

None declared.

Submitted 01 May 2020
Revised 10 September 2020
Accepted 14 November 2020

Associate editor: Thomas Kiørboe